Frontiers of Information Technology & Electronic Engineering
www.jzus.zju.edu.cn; engineering.cae.cn; www.springerlink.com
ISSN 2095-9184 (print); ISSN 2095-9230 (online)
E-mail: jzus@zju.edu.cn

Development of an onsite calibration device for robot manipulators*#

Ziwei WAN[1,2], Chunlin ZHOU‡[1,3], Haotian ZHANG[4], Jun WU[1]

[1]*College of Control Science and Engineering, Zhejiang University, Hangzhou 310063, China*
[2]*Huzhou Institute of Zhejiang University, Huzhou 313098, China*
[3]*Binjiang Institute of Zhejiang University, Hangzhou 310014, China*
[4]*School of Information and Software Engineering, University of Electronic Science and Technology of China, Chengdu 610054, China*

E-mail: wanzw@zju.edu.cn; c_zhou@zju.edu.cn; zhanghtpex@163.com; junwuapc@zju.edu.cn

Received Apr. 27, 2022; Revision accepted Sept. 4, 2022; Crosschecked Dec. 6, 2022

Abstract: A novel in-contact three-dimensional (3D) measuring device, called MultiCal, is proposed as a convenient, low-cost (less than US$5000), and robust facility for onsite kinematic calibration and online measurement of robot manipulator accuracy. The device has μm-level accuracy and can be easily embedded in robot cells. During the calibration procedure, the robot manipulator first moves automatically to multiple end-effector orientations with its tool center point (TCP) constrained on a fixed point by a 3D displacement measuring device (single point constraint), and the corresponding joint angles are recorded. Then, the measuring device is precisely mounted at different positions using a well-designed fixture, and the above measurement process is repeated to implement a multi-point constraint. The relative mounting positions are accurately measured and used as prior information to improve calibration accuracy and robustness. The results of theoretical analysis indicate that MultiCal reduces calibration accuracy by 10% to 20% in contrast to traditional non-contact 3D or six-dimensional (6D) measuring devices (such as laser trackers) when subject to the same level of artificial measurement noise. The results of a calibration experiment conducted on a Staubli TX90 robot show that MultiCal has only 7% to 14% lower calibration accuracy compared to a measuring arm with a laser scanner, and 21% to 30% lower time efficiency compared to a 6D binocular vision measuring system, yielding maximum and mean absolute position errors of 0.831 mm and 0.339 mm, respectively.

Key words: Calibration device; Kinematic calibration; Onsite calibration; Absolute accuracy
https://doi.org/10.1631/FITEE.2200172 **CLC number:** TP242.2

1 Introduction

With an ever-increasing demand for higher accuracy, metrology devices and methods for kinematic calibration of robot manipulators have progressed tremendously over the past three decades (Chen et al., 2020). These calibration systems have been shown to effectively reduce the absolute position errors of robot manipulators, which can be caused by many factors, such as manufacturing tolerance,

‡ Corresponding author
* Project supported by the Key R&D Program of Zhejiang Province, China (No. 2022C04030), the National Key R&D Program of China (Nos. 2020YFB1313300 and 2018AAA0102703), and the National Natural Science Foundation of China (No. 61836015)
# Electronic supplementary materials: The online version of this article (https://doi.org/10.1631/FITEE.2200172) contains supplementary materials, which are available to authorized users
ORCID: Ziwei WAN, https://orcid.org/0000-0002-3717-187X; Chunlin ZHOU, https://orcid.org/0000-0001-6939-9732

assembling error, and structural deformation (Feng et al., 2009). Robots with offline programming or autonomous path planning capabilities especially benefit from these calibration systems, because the absolute accuracy of a robot, rather than its higher repeatability, ensures that the motion instructions calculated in simulation environments can be directly used for real tasks. In general, the application cases of these calibration systems can be roughly classified into three categories, large-batch calibration by professional robot manufacturers, small-batch calibration by robot developers and researchers, and routine maintenance and recalibration by robot users.

For the case of routine maintenance and recalibration, as presented in Fig. 1, it is desired to have an accurate and convenient calibration device that can be easily embedded into the worksite or product line where the robot is located. Because the robot accuracy keeps deteriorating over time (Qiao and Weiss, 2017), the device should preferably be able to measure and monitor the robot's accuracy automatically during the robot's intermission (see supplementary materials, Section 1). If the accuracy severely deteriorates, the device will stop the operation process and give an alarm to inform users to calibrate the robot directly at its worksite (onsite calibration). In summary, in contrast to in-house calibration of professional robot manufacturers, the requirements for this application case are quite different. The device must be highly accurate, low-cost, easily operated, robust, portable, and easily deployed in robot cells. Note that fully automated calibration is unnecessary in this case, because frequent calibrations are not required and manual interventions must be involved.

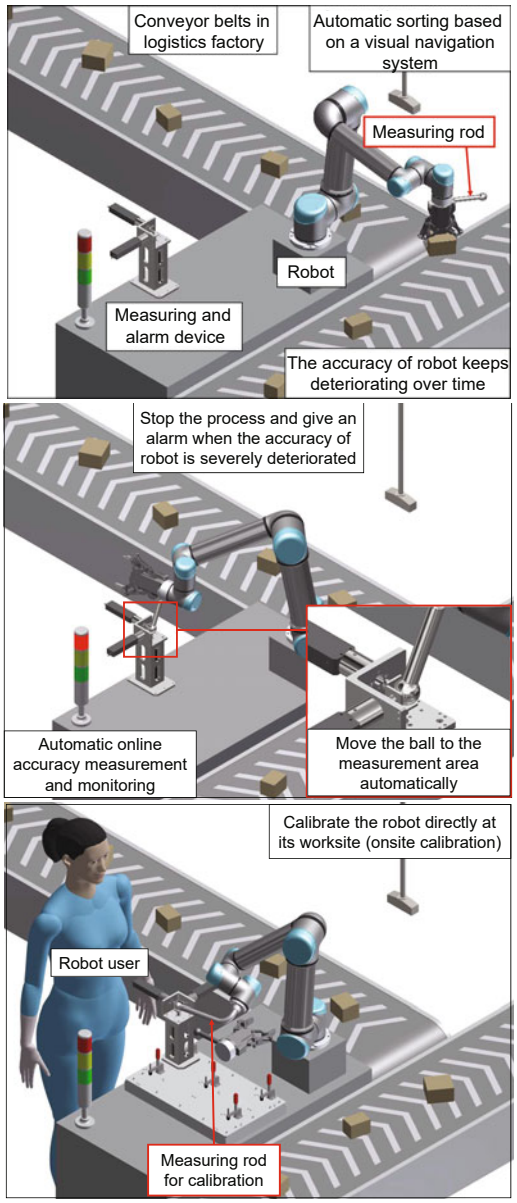

Fig. 1 Application case of online accuracy measurement and onsite calibration in a logistics factory

However, traditional calibration devices such as laser trackers (Sun T et al., 2016), laser interferometers (Castro and Burdekin, 2006), mechanical coordinate measuring machines (CMMs) (Cong et al., 2006), and optical CMMs (Nubiola et al., 2014) can hardly be used in these cases because they are easily restricted by the working environment and are too expensive (more than US$30 000). Alternatively, many portable and low-cost calibration devices with good environmental adaptability have been developed. The one-dimensional (1D) measuring device based on a single wire draw encoder (Zhan, 2015) or a single laser displacement sensor (Guo et al., 2020) can be used for fully automated calibration without manual intervention. However, parameter identification based on 1D measurements is relatively poor in accuracy and robustness, because the robot's accuracy before calibration must be high; otherwise, it will easily fall into a local optimum. Hence, 3D or 6D measuring devices consisting of multiple wire draw encoders (Legnani and Tiboni, 2014) were proposed to solve this problem, but these systems are relatively complex and expensive. Eye-in-hand devices based on optical sensors (ROSY by Teconsult GmbH) or cameras (Enebuse et al., 2021) may be another solution for such scenarios because they are affordable and easy to implement, but the effectiveness

of eye-in-hand devices is still challenged when comparing the end-result accuracy obtained through external devices (Icli et al., 2020). Calibration systems based on touch probes (Zhong et al., 1996), standard balls (Joubair and Bonev, 2015), and standard blocks (Ikits and Hollerbach, 1997) are low-cost and easy to fabricate, but the measurement process of these systems needs a repeated manual back-and-forth adjustment, which is very time-consuming and will easily damage the probe. In conclusion, these measuring devices still cannot meet the requirements of the above application scenarios.

Perhaps the best solution for this case is the widely used measurement strategy in robot calibration that constrains the robot's tool center point (TCP) to a fixed point in space using displacement sensors, since displacement sensors are inherently low in price, have good environmental adaptability, and can measure within a certain measurement range (10 mm or larger), which is conducive to robot automatic measurement without collision. However, if only a single point constraint is adopted (or the TCP is measured only within a small area, such as LaserLAB of Wiest AG), the calibration result will also be very sensitive to the initial kinematic parameters, and will easily get stuck at locally optimal values.

To overcome this shortcoming, calibration devices based on multi-point constraints are proposed. A representative of this type is TriCal (Gaudreault et al., 2016), which can be mounted on the robot's end-effector and the robot can be calibrated by probing a set of balls. The relative positions of the balls are precisely measured and used as prior information, which significantly increases the accuracy and robustness of parameter identification. However, TriCal can hardly be used for calibrating small robots due to its large volume. On the other hand, the motion space of the robot will be seriously limited, leading to insufficient calibration accuracy in the whole robot workspace, especially for large robots.

In this work, we develop a new in-contact onsite calibration device called MultiCal (multi-position calibration) based on a measuring rod, a 3D displacement measuring device, and a multi-position fixture (Fig. 2). In contrast to TriCal, the mounting positions of the ball and the 3D displacement measuring device are reversed. A light and long measuring rod, rather than an entire measuring device, is installed at the robot's end-effector, which has four advantages. First, the measuring rod is clearly longer, which allows the robot to move in a larger space, and eventually attains high calibration accuracy and robustness in the whole robot workspace. Second, since the measuring rod can also be made smaller and lighter (weighing less than 0.3 kg for short rods), our device is more suitable for calibrating small-sized or low-stiffness robots. Third, given that the measuring device is not installed on the robot's end-effector, we apply three larger and heavier displacement sensors with a larger measurement range (30 mm), which makes the system easier to operate and less prone to collision. Finally, unlike TriCal's 3D artifact, the high-rigidity multi-position fixture has no vulnerable components that are critical to system accuracy (such as ball stems), making the system more robust and its accuracy easier to maintain. The latter two advantages are especially important for non-professional users who are more likely to operate the device incorrectly.

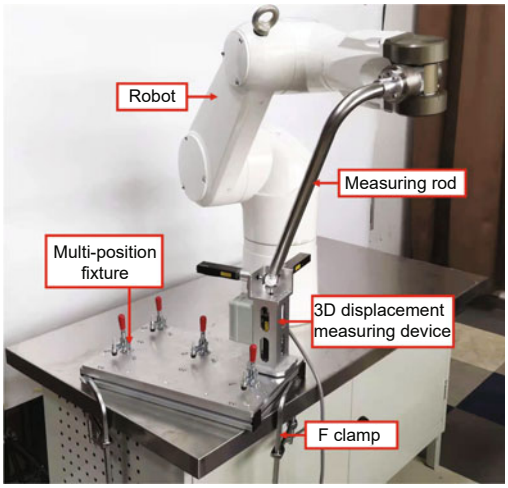

Fig. 2 A new in-contact onsite calibration device called MultiCal

2 Calibration device

In this section, the MultiCal system components, including a measuring rod, a 3D displacement measuring device, and a multi-position fixture, are presented in detail. Then, the measurement accuracy of this system is comprehensively evaluated.

As illustrated in Fig. 3, the measuring rod is designed as a modular tool that can be easily customized and fabricated at a low cost. A high-precision ceramic ball (diameter of 25 mm to 60 mm)

is attached to a ball holder and connected with a pipe holder via a stainless steel bending pipe (diameter of 20 mm to 50 mm) using two threaded connectors. The bending pipe can be designed in different sizes and shapes, while the pipe holder can be designed for different robot flanges. The cost of customizing this measuring rod is very low, since it does not require high-level dimension tolerance, but only high rigidity. Furthermore, the ball holder and the pipe holder can be easily replaced using the threaded connectors, and only the bending pipe needs to be remade, which costs less than US$100. To guarantee high rigidity, the diameters and thicknesses of the bending pipe and the threaded connectors need to be increased as the rod's length increases. The measuring rod has three parameters, i.e., the lengths and included angle of the first and second pipe segments, or l_1, l_2, and γ. The corresponding coordinates of the ballą́s center with respect to (w.r.t.) the robot flange frame (tool parameter) are

$$\begin{cases} x_{\text{tool}} = l_2 \sin\gamma, \\ y_{\text{tool}} = 0, \\ z_{\text{tool}} = l_1 - l_2 \cos\gamma. \end{cases} \tag{1}$$

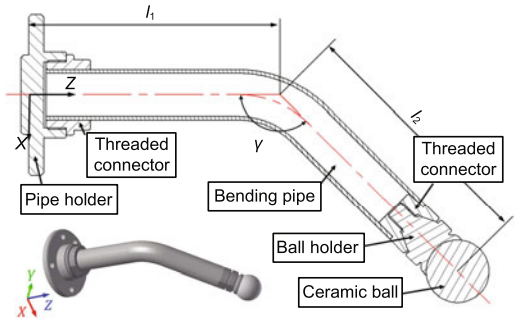

Fig. 3 Description of the measuring rod

As illustrated in Fig. 4, three displacement sensors (ONOSOKKI GS-4830, measurement range of 30 mm, resolution of 1 μm, accuracy of 3 μm) are fixed orthogonally in the triaxial mount and measure the real-time XYZ displacements of the ball's center when the ball is in contact with the three square-shaped tips. The aluminum triaxial mount is manufactured by CNC Precision Machining to ensure the verticality of the three displacement sensors' axes (better than 0.05 mm). The fixing sleeve closely matches the cylindrical mounting surface of each sensor to guarantee high coaxiality. A cylindrical pin with a round head protrudes from each inner face of the triaxial mount as a physical stopper. Before measurement, each square-shaped tip is pushed manually to touch the physical stopper as the zero position of the displacement sensor. The overall weight of the 3D measuring device is 3.4 kg.

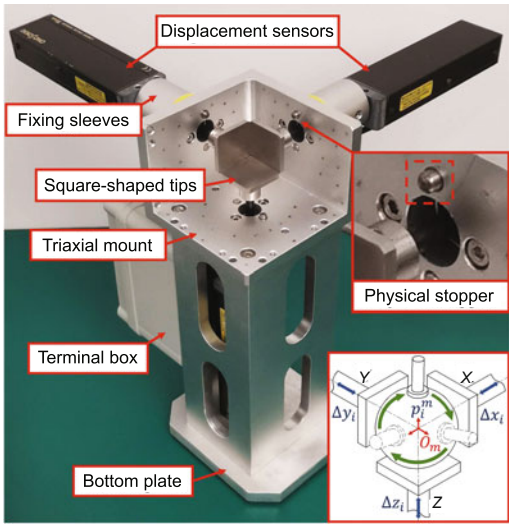

Fig. 4 Description of the 3D displacement measuring device

To increase measurement diversity and implement a multi-point constraint, we employ a multi-position fixture (Fig. 5) to provide five different mounting positions for measurement, which can be regarded as five virtual point constraints (see Section 2 of the supplementary materials for the reasons why we set five mounting positions). The multi-position fixture is composed of an aluminum top plate, an aluminum bottom frame, and five sets of well-designed fast-lock mechanisms (Fig. 6). Using a toggle clamp, the 3D measuring device can be quickly mounted on different mounting positions (less than 15 s) with three sets of cylindrical pins and double balls guaranteeing the assembly accuracy. Both the cylindrical pins and balls are made of tungsten steel with a high degree of hardness (HRA 93). The relative mounting positions $\left[P_x^j, P_y^j, P_z^j\right]$ $(j = 1, 2, \ldots, 5)$ are precisely measured by a Hexagon RA8520-7 coordinate measuring arm (measurement accuracy of 20 μm) and PolyWorks$^{\text{TM}}$ (see Section 3 of the supplementary materials for the specific measurement method), as shown in Table 1. Because the multi-position fixture is highly rigid, these parameters can be used for a long time once they are measured, so the do-it-yourself (DIY) difficulty and cost

will not be too large (measuring arms or CMMs can be rented). Additionally, the multi-position fixture can be easily carried and embedded in robot cells, because its overall size is 500 mm×300 mm×151 mm, and its overall weight is 7.1 kg.

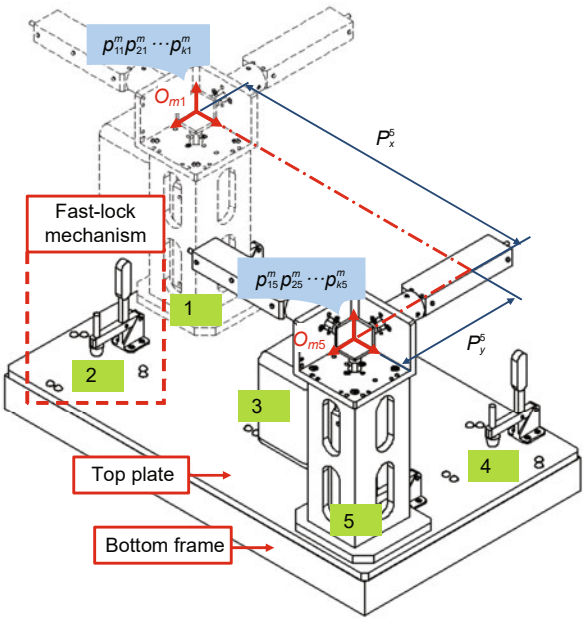

Fig. 5 Description of the multi-position fixture and its five mounting positions

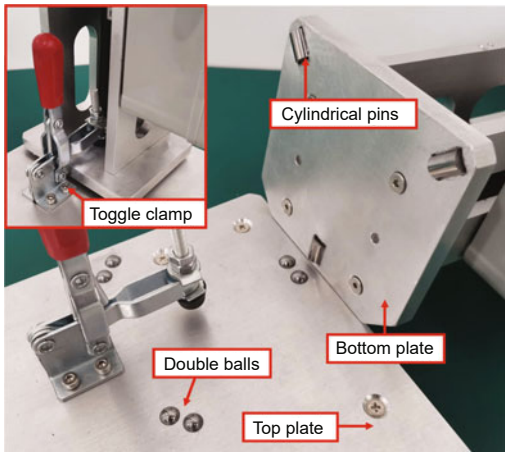

Fig. 6 Close-up of the fast-lock mechanism

During the calibration procedure, we first mount the 3D measuring device on the multi-position fixture and manually reset the zero positions of the three displacement sensors with the method described above. Then we adjust the robot to (almost) align the ball's center to a fixed point (virtual datum point) of the 3D measuring device with k different end-effector orientations. The virtual datum point is a point 15 mm away from the zero position of each sensor (the distance can be adjusted according to the ball's diameter). This process can be realized by a semi-automatic or fully automatic approach, as described in Section 4 of the supplementary materials. Considering various errors and disturbances, there will still be very small XYZ displacements of the ball's center w.r.t. the virtual datum point after the alignment of the point. Then, we manually mount the 3D measuring device in different mounting positions and repeat the above measurement process p times to ultimately obtain the small XYZ displacements $\left[\Delta x_i^j, \Delta y_i^j, \Delta z_i^j\right]$ $(i = 1, 2, \ldots, k, j = 1, 2, \ldots, p)$ and the corresponding joint angles $\boldsymbol{q}_i^j$ $(i = 1, 2, \ldots, k, j = 1, 2, \ldots, p)$. We establish a world reference frame $\{W\}$ as a measuring device frame with its origin as the virtual datum point of mounting position 1, and its XYZ axes are (almost) parallel to the axes of the corresponding displacement sensors. Considering that the parallelism errors between the XYZ sensors' axes of the measuring device in different mounting positions are all measured as less than 0.1 mm, and the ball's center almost coincides with the virtual datum point during the measurement, the small XYZ displacements can be added directly to the XYZ position offsets of different mounting positions in Table 1, respectively, to obtain the measured position of the balls' center $\boldsymbol{p}_{ij}^m$ w.r.t. $\{W\}$, namely

Table 1 The relative positions of the five mounting positions

	Relative position (mm)				
	1	2	3	4	5
P_x	0	164.796	83.911	2.836	167.969
P_y	0	−1.234	191.802	384.875	384.015
P_z	0	−0.295	−0.584	−0.434	−1.195

$$\boldsymbol{p}_{ij}^m = \begin{bmatrix} P_x^j + \Delta x_i^j \\ P_y^j + \Delta y_i^j \\ P_z^j + \Delta z_i^j \end{bmatrix} \begin{pmatrix} i = 1, 2, \ldots, k \\ j = 1, 2, \ldots, 5 \end{pmatrix}. \quad (2)$$

A measurement accuracy assessment for Multi-Cal is carried out. First, the sphericity and diameter tolerance of the precision ceramic ball used in this work are tested better than 2 μm using an indicator. Then, because a perfect TCP alignment is almost realized, the 3D measuring device needs only high

repeatability, rather than high accuracy. Hence, the accuracy of the displacement sensors (even though the accuracy is 3 μm in this work) and the machining and assembly accuracy of the measuring device are not required to be very high.

The assembly error of the fast-lock mechanism is also strictly evaluated. A repetitive mounting test is conducted five times on each mounting position, and the repetitive assembly error is measured using the Hexagon measuring arm with the same methods described in Section 3 of the supplementary materials. The results show that the maximum and mean assembly errors are 35 μm and 17.2 μm, respectively. Hence, even if we consider the wear of the cylindrical pins and balls, and the slight deflection of the multi-position fixture, the measurement accuracy of MultiCal is still several times the absolute positioning accuracy that current robot manipulators can achieve.

3 Calibration algorithm

This section details the kinematic calibration algorithm and the selection algorithm for optimal measurement configurations used for MultiCal.

Before the calibration procedure, the precision ball's center is defined as the robot's TCP. When a point cloud of the actual TCP w.r.t. the measuring device frame $\{W\}$ is accurately measured, and a point cloud of the nominal TCP w.r.t. the robot base frame $\{0\}$ is calculated using forward kinematics, the point cloud registration from $\{W\}$ to $\{0\}$ can be achieved. After that, the errors of modified Denavit-Hartenberg (MDH) parameters can be identified through error backpropagation using the Jacobian matrix.

Let $\boldsymbol{p}^n$ be the nominal position vector of the ball's center (TCP) w.r.t. the robot base frame $\{0\}$. Based on the forward kinematic equation, $\boldsymbol{p}^n$ can be written as

$$\boldsymbol{p}^n = f(\boldsymbol{q}, \boldsymbol{e}), \tag{3}$$

where $\boldsymbol{q}$ is the robot joint angle vector and $\boldsymbol{e}$ is the error vector of the kinematic parameters. Denote the matrices composed of the nominal position vectors $\boldsymbol{p}_{ij}^n$ and the measured position vectors $\boldsymbol{p}_{ij}^m$ as $[\boldsymbol{p}^n]$ and $[\boldsymbol{p}^m]$ respectively, and the robot base and world reference frame transformation matrix as $\boldsymbol{T}_1$. Then, $\boldsymbol{T}_1$ can be roughly calculated using the least-squares method:

$$\boldsymbol{T}_1 = \left[\boldsymbol{R}_1 \ \boldsymbol{t}\right] = [\boldsymbol{p}^n]\,[\boldsymbol{p}^m]^{\mathrm{T}} \left([\boldsymbol{p}^m]\,[\boldsymbol{p}^m]^{\mathrm{T}}\right)^{-1}, \tag{4}$$

where $\boldsymbol{R}_1$ is regarded as the 3×3 rotation matrix and $\boldsymbol{t}$ is the translation vector of $\boldsymbol{T}_1$. Due to errors, $\boldsymbol{R}_1$ is a strict orthogonal matrix. Hence, the Lagrangian multiplier method (Li and Shen, 1991) is used to orthogonalize $\boldsymbol{R}_1$:

$$\boldsymbol{R}_2 = \left(\boldsymbol{R}_1\boldsymbol{R}_1^{\mathrm{T}}\right)^{-\frac{1}{2}}\boldsymbol{R}_1. \tag{5}$$

Then, $\boldsymbol{R}_2$ and $\boldsymbol{t}$ are recombined to obtain a new frame transformation matrix $\boldsymbol{T}_2 = [\boldsymbol{R}_2 \ \ \boldsymbol{t}]$. After that, let $\boldsymbol{p}_{ij}^r$ be the measured position vector of the ball's center w.r.t. the robot base frame $\{0\}$. Then, $\boldsymbol{p}_{ij}^r$ can be obtained using $\boldsymbol{T}_2$, namely

$$\boldsymbol{p}_{ij}^r = \boldsymbol{T}_2\boldsymbol{p}_{ij}^m. \tag{6}$$

For simplicity, we convert matrix $\boldsymbol{T}_2$ to the 6D pose vector $\boldsymbol{x}_2$, namely

$$\boldsymbol{T}_2 = \boldsymbol{T}(x, y, z, Rz, Ry, Rx) = \boldsymbol{T}(\boldsymbol{x}_2). \tag{7}$$

Denote the difference vector between the real position vector $\boldsymbol{p}^r$ and the nominal position vector $\boldsymbol{p}^n$ as $\Delta\boldsymbol{p}$. According to a previous work (Luo et al., 2021), $\Delta\boldsymbol{p}$ has an approximately linear relationship with the error vector of the kinematic parameters $\boldsymbol{e}$ in Eq. (3). In other words, there is a Jacobian matrix $\boldsymbol{J}$:

$$\Delta\boldsymbol{p} = \boldsymbol{p}^r - \boldsymbol{p}^n = \boldsymbol{J}\boldsymbol{e}. \tag{8}$$

Denote the error vector and the Jacobian matrix composed of $\Delta\boldsymbol{p}_{ij}$ and $\boldsymbol{J}_{ij}$ at different measurement configurations as $[\Delta\boldsymbol{p}]$ and $[\boldsymbol{J}]$, respectively. Then, $\boldsymbol{e}$ can be identified with the least-squares method:

$$\boldsymbol{e} = \left([\boldsymbol{J}]^{\mathrm{T}}[\boldsymbol{J}]\right)^{-1}[\boldsymbol{J}][\Delta\boldsymbol{p}]. \tag{9}$$

Since both $\boldsymbol{e}$ and $\boldsymbol{x}_2$ have errors, we further optimize them together using the Levenberg-Marquardt (LM) algorithm, which is a robust non-linear optimization algorithm widely used in robot kinematics, as presented in Eq. (10):

$$(\boldsymbol{e}, \boldsymbol{x}) = \arg\min \sum_{i=1}^{k}\sum_{j=1}^{p} \left\| T(\boldsymbol{x})\left[\boldsymbol{p}_{ij}^m\right] - f\left(\boldsymbol{q}_{ij}, \boldsymbol{e}\right)\right\|^2. \tag{10}$$

Note that MultiCal does not need to be accurately mounted in an expected position w.r.t. the

robot base, since the 6D pose vector $\boldsymbol{x}$ of the measuring device frame $\{W\}$ w.r.t. the robot base frame $\{0\}$ and the MDH parameter errors $\boldsymbol{e}$ will be identified at the same time.

For the LM algorithm, the observability index (OI) of the Jacobian matrix in the optimization can be used for evaluation. If the OI value is large, it means that the influence of unmodeled errors on the parameter identification is small, resulting in high calibration accuracy and robustness. In this work, the observability index O_1 (Sun Y and Hollerbach, 2008) is used, where a previous study showed better results compared to other OI equations (Joubair et al., 2013). The equation is presented as

$$O_1 = \frac{\sqrt[m]{\sigma_1\sigma_2\dots\sigma_m}}{\sqrt{n}}, \tag{11}$$

where σ_i's $(i = 1, 2, \dots, m)$ are the singular values of the identification Jacobian matrix, m is the number of calibration parameters, and n is the number of measured configurations. The objective of O_1 is to maximize the product of the singular values, which means increasing the volume of the ellipsoid. Based on this, we first generate a large pool of feasible configurations that are reachable, measurable, and free of collision through a simulation in RoboDK and MATLAB, and then select the optimal set of configurations for parameter identification using the DETMAX algorithm (Mitchell, 1974).

4 Simulation

In this section, we first establish the robot kinematic model, and then describe the simulation procedure for obtaining the optimal measurement configurations. Based on this, we choose the optimal parameters of the measuring rod through an OI evaluation, and finally challenge MultiCal against four traditional calibration methods in a simulation comparison.

4.1 Kinematic model of the robot

In theory, MultiCal can be used to calibrate different kinds of robots (including SCARA, Delta, parallel robot, and robots with special joint configurations). Among them, we take a Staubli TX90 robot (Fig. 7, repeatability of 0.03 mm), which is a standard 6-axis serial robot, as an example to test MultiCal's performance. The first step is to establish the kinematic model of the robot with a measuring rod installed at its end. The center of the precision ball is defined as the origin of the tool frame (TCP).

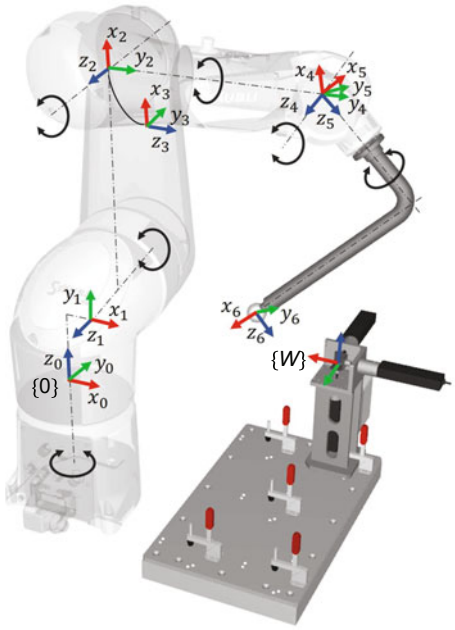

Fig. 7 The modified Denavit-Hartenberg (MDH) model of the Staubli TX90 robot

There are many kinematic modeling methods for articulated serial robots, such as Denavit-Hartenberg (DH), modified DH (MDH) (Hayati and Mirmirani, 1985), product of exponential (POE) (Park and Okamura, 1994), and finite and instantaneous screw (FIS) (Sun T et al., 2020). The DH method is straightforward and easy to understand, but it will have a singular problem when two neighboring joints are parallel or nearly parallel. The MDH method solves this problem by adding a rotation angle β around the y axis, but special attention is needed for assigning body-fixed frames and elimination of redundant errors (Sun T et al., 2020). Both the POE and FIS methods can establish a continuous model and describe kinematic errors in a straightforward manner, which simplifies the modeling process. However, a deep understanding of the mathematical background is required to implement these methods. On the other hand, previous works (Sun T et al., 2020) proved that the MDH method will obtain the same effect as the POE and FIS methods if the redundant errors can be correctly removed. Therefore, we adopt the easy-to-use MDH method, remove the redundant errors, and eventually determine the

MDH parameters and their 21 corresponding error terms $\boldsymbol{e}$, as presented in Table 2.

Note that no error terms are set for θ_1 and d_1, because they are coupled with the 6D pose vector $\boldsymbol{x}$ of the world reference frame $\{W\}$ w.r.t. the robot base frame $\{0\}$. However, we can still improve the robot's accuracy or even perform offline programming, because the tool and workpiece reference frame parameters can be calibrated using other standard methods before actual use.

Additionally, we need to measure at least 10 robot configurations to make the number of constraints more than the number of parameters that need to be identified $(21+6)$, since each measured configuration can produce three constraints (in X, Y, and Z directions).

4.2 Simulation procedure

In the simulation, a large pool of feasible robot joint sets (reachable, measurable, and free of collision) is generated using the following method. First, keeping the point constraint of the ball's center, we uniformly distribute the end axis of the measuring rod on the 1/8 spherical open area of the 3D measuring device (Fig. 8). Specifically, the orientations of the end axis are characterized by the concept of latitudes and longitudes in geography. The angle between every two adjacent latitudes is 15°, while the angle between every two adjacent axes at the same latitude is 15°. The measuring rod is rotated around its end axis with an interval of 30° to obtain a large set of final end-effector orientations. Then the corresponding set of robot configurations is solved using inverse kinematics, and the above process is repeated on different mounting positions. Finally, we eliminate the joint angle sets that exceed limits, are in the singular region, or have a static or dynamic collision during the automatic orientation adjustment, and then add the remaining configurations to the pool. After that, the optimal n measurement configurations and the corresponding OI values are obtained with the DETMAX algorithm.

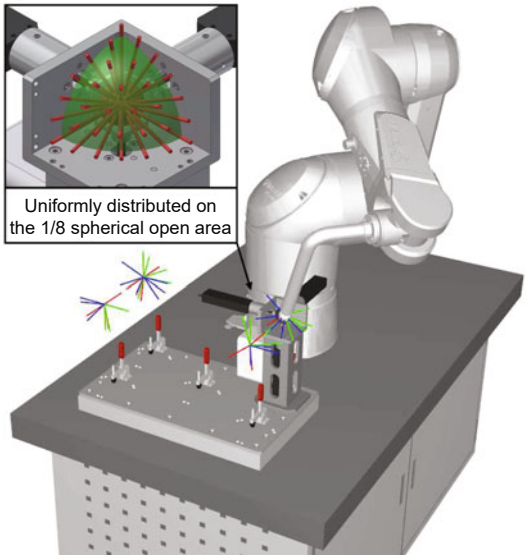

Fig. 8 Selecting the optimal set of measurement configurations based on an observability index evaluation in MATLAB and RoboDK

Note that the parameters of the measuring rod (l_1, l_2, and γ) and the placement position of the multi-position fixture will affect the performance of the calibration system. Therefore, the optimal values of these parameters are also determined through a simulation, which is detailed in Section 5 of the supplementary materials due to space limitations. The results show that the measuring rod would attain the best performance when l_1=350 to 425 mm, l_2=575 to 650 mm, and $\gamma = 90°$ in a virtual environment. The lengths of links 1–2 and 3–4 of the Staubli TX90 are both 425 mm, which means that the theoretical optimal l_1 and l_2 are 80% to 100% and 135% to 145% of the length of the robot links respectively, and the theoretical optimal γ is 90°, which provides design guidance for the measuring

Table 2 The MDH parameters of the Staubli TX90 robot

Link	θ (°)	d (mm)	a (mm)	α (°)	β (°)
0–1	θ_1	150	$50+\delta a_1$	$90+\delta\alpha_1$	0
1–2	$\theta_2+90+\delta\theta_2$	$-50+\delta d_2$	$425+\delta a_2$	$0+\delta\alpha_2$	$0+\delta\beta_2$
2–3	$\theta_3+90+\delta\theta_3$	0	δa_3	$90+\delta\alpha_3$	0
3–4	$\theta_4+\delta\theta_4$	$425+\delta d_4$	δa_4	$-90+\delta\alpha_4$	0
4–5	$\theta_5+\delta\theta_5$	δd_5	δa_5	$90+\delta\alpha_5$	0
5–6	$\theta_6+\delta\theta_6$	$z_{\text{tool}}+100+\delta d_6$	$x_{\text{tool}}+\delta a_6$	0	0

rods used for differently sized robots. Note that the measuring rod is regarded as an absolute rigid body in the simulation, without considering rod deflections. This means that a longer rod often has better calibration performance, because it makes the robot move in a larger space. However, in the real environment, if a measuring rod is too long, the deflection of the rod caused by the effects of gravity will be very serious, which will reduce the measurement accuracy. This means that we need to find a balance between rod rigidity and robot motion space, which is further studied in Section 5.

As for the optimal placing position of the multi-position fixture, the simulation results show that placing the fixture horizontally beside the robot with the nearest distance between the fixture and robot axis 1 being about 300 to 450 mm can attain the highest OI value. The optimal height of the measuring device frame $\{W\}$ w.r.t. the robot base frame $\{0\}$ is about –200 to 100 mm, which is determined by the rod length. Normally, the longer the rod, the lower the fixture that needs to be placed.

In simulation, we also compare MultiCal with other calibration methods at a theoretical level. The traditional methods based on non-contact 3D measuring (3DM) devices (such as a laser tracker and a single spherically mounted retroreflector (SMR)) (Sun T et al., 2016), 6D measuring (6DM) devices (such as a laser tracker with a triangular artifact and three SMRs) (Nubiola et al., 2014), 1D measuring (1DM) devices (such as a single wire draw encoder) (Zhan, 2015), and the circular point analysis (CPA) method (Cho et al., 2019) are taken as representatives. The experiments are detailed in Section 6 of the supplementary materials. The results show that the theoretical calibration accuracy of MultiCal is indeed lower (about 10% to 20%) than that of the traditional 6D and 3D measuring devices when the measuring devices have the same level of measurement accuracy. However, compared with traditional devices, MultiCal can achieve higher measurement accuracy more easily and at a lower cost. This means that it can eventually achieve calibration accuracy similar to or even better than those of traditional devices, which is also proved in Section 5. Additionally, the method based on 1DM devices and the CPA method have the worst performance in the experiments, with 60% to 70% lower calibration accuracies compared to MultiCal.

5 Calibration experiments on the Staubli TX90 robot

The following section describes the calibration experiments conducted on a Staubli TX90 robot, including an effectiveness validation of MultiCal, a comparison between measuring rods of different sizes and shapes, and a comprehensive comparison between MultiCal and two other traditional measuring devices in terms of calibration accuracy, time efficiency, and device cost.

Initially, as illustrated in Fig. 2, the multi-position fixture was fixed on the workbench with the nearest distance between the fixture and axis 1 of the robot being 400 mm. Then, the measuring rods with l_1–l_2–γ of 125–500–90 and 125–200–90 were chosen as the representatives of long rods and short rods, respectively, and their corresponding optimal 30 measurement configurations were generated according to the experiment setup. After that, a measurement procedure with a fully automatic adjustment based on off-line programming in RoboDK was conducted.

After that, the MultiCal system was removed, and a measuring arm with a Hexagon AS1 laser scanner (Fig. 9, the overall accuracy of the scanning system was 43 μm) was used to conduct a traditional calibration procedure based on 3DM. The robot was sent to 30 joint sets, which were optimized based on the same OI as above; the only constraints were to avoid collisions and have the precision ceramic ball in the measurement space of the laser scanner. Then we manually scanned the ball (at least 60% of its surface), conducted a spherical fitting of the obtained point cloud, and exported the coordinates of the ball's center using PolyWorks. Different sets of MDH parameters were then identified separately with the measurement data obtained from different measuring devices.

It is worth mentioning that although the measuring arm with a laser scanner is not suitable for robot calibration due to its low time efficiency (it needs to scan manually every time) and small measurement volume, it is very suitable for the validation of MultiCal, because it can directly obtain the coordinates of the TCP (the ball's center) without replacing the ceramic ball with other measuring markers (such as SMRs). Hence, there is no need to design a kinematic coupling mechanism like TriCal, and the TCP deviations caused by it can

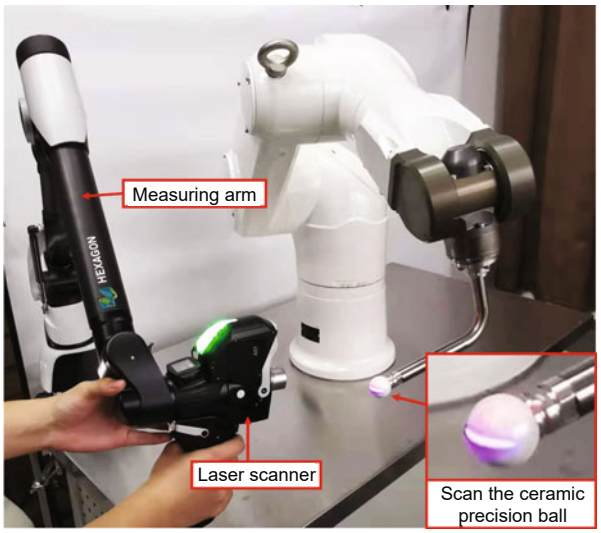

Fig. 9 Using a measuring arm with a laser scanner for validation and conducting the traditional calibration procedure based on 3D measuring (3DM) devices

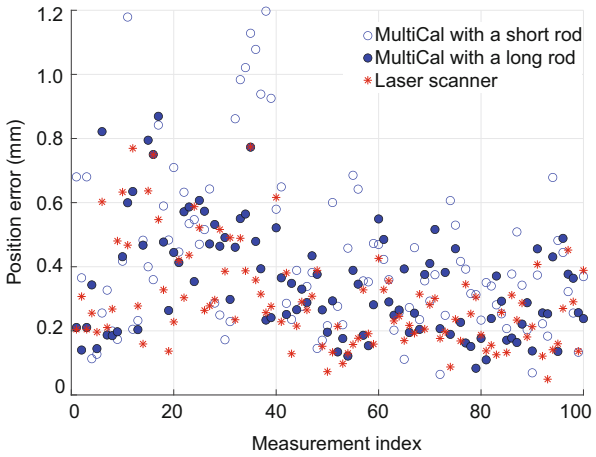

Fig. 10 Absolute position errors of the robot calibrated using MultiCal and the laser scanner

be avoided. Additionally, the measurement is non-contact, so there is no measurement error caused by contact force.

After the calibration was completed, with the same measurement method as above, the laser scanner was used to measure 100 random robot configurations within the whole robot workspace as validation data. Considering that the measurement volume of the laser scanner was more limited, the measurement diversity of the validation data was worse than that of the data collected by a laser tracker with the ISO standard method (ISO, 1998). However, the validation data used in this work also covered a very large portion of the whole workspace, especially when using a long measuring rod.

Based on the joint angle sets in the validation data, different sets of nominal TCPs were calculated with different sets of MDH parameters. Then the corresponding frame transformation matrix was obtained using the method mentioned in Section 3, and the measured TCPs w.r.t. the robot base frame {0} were calculated. After that, the distance errors between the nominal TCPs and the measured TCPs were calculated as the robot's absolute position errors (Fig. 10). Before the experiment, the mean and maximum position errors of the robot were measured as 2.211 and 6.245 mm, respectively.

The results showed that MultiCal can significantly improve the absolute positioning accuracy of the robot, yielding mean position errors of 0.348 and 0.427 mm, and maximum position errors of 0.869 and 1.197 mm for the cases of long and short rods, respectively. The calibration accuracy of MultiCal with the long rod was only slightly worse (7.91%) than that of the 3DM method using the laser scanner. This means that the measurement accuracy of MultiCal is very high. In contrast to the short rod, the position error distribution obtained by the long rod was more uniform, which indicates that the robot accuracy in the whole workspace is higher, proving the unique advantages of the long measurement rod. This characteristic is quite different from most other similar in-contact calibration devices, where the high positioning accuracy appears only in the workspace near the measurement area.

A comparative experiment between more measuring rods of different sizes and shapes was also conducted (Fig. 11). According to the simulation results described in Section 5 of the supplementary materials, for the case of $\gamma = 90°$, the measuring rods with l_1–l_2 of 125–200, 125–350, 125–500, 275–425, and 425–650 were chosen as representatives. The measuring rods with l_1–l_2 of 100–100, 150–150, 200–200, 250–300, and 350–450 were chosen for the case of $\gamma = 135°$. The optimal measurement configurations for these 10 measuring rods were selected separately, and the same measurement and validation procedures described above were carried out; the results are presented in Table 3.

In the real environment, the measuring rod with l_1–l_2–γ being 125–500–90 rather than 425–650–90 or 275–425–90 had the best calibration performance, although the latter two attained higher OI values in the

Fig. 11 Measuring rods of different sizes and shapes tested in the comparative experiment

Table 3 The highest observability index (OI) and calibration results obtained with different measuring rods

Measuring rod (l_1–l_2–γ)	OI	Mean (mm)	Max (mm)	Median (mm)	Standard deviation (mm)
125–200–90	1.432	0.427	1.197	0.363	0.252
125–350–90	1.604	0.401	0.912	0.358	0.243
125–500–90	**1.716**	**0.348**	**0.869**	**0.296**	**0.156**
275–425–90	1.828	0.462	1.168	0.435	0.214
425–650–90	1.937	0.518	1.325	0.420	0.296
100–100–135	0.975	0.962	2.469	0.850	0.543
150–150–135	1.341	0.520	1.460	0.411	0.320
200–200–135	1.473	0.410	1.085	0.364	0.252
250–300–135	1.595	0.406	0.928	0.362	0.241
350–450–135	1.654	0.431	1.232	0.385	0.268

The bold number indicates the best performance

simulation. The same phenomenon occurred on the longest two measuring rods when $\gamma = 135°$. A possible reason is the deflection of the long rod caused by the effects of gravity on the rod itself, which will increase rapidly as the rod's length increases, leading to a position deviation of the ball's center and bringing unmodeled errors to the measurements. Hence, it is necessary to design a more rigid structure for the measuring rods or propose a method to compensate for this deflection in future work, especially for the calibration of larger robots. From another perspective, when mounting a measuring device at the end of a robot (such as TriCal), it is harder to achieve the same pleasing performance as MultiCal by increasing the length of the device's mounting bracket. This is because the heavier measuring device will greatly enlarge this kind of deflection.

However, when the measuring rod was not that long, and the rod deflection error was not the dominant error source, then the measuring rod with a higher OI value yielded a better calibration result. Additionally, as in the simulation results, the calibration accuracies obtained by the measuring rods with $\gamma = 135°$ were generally lower than those of the rods with $\gamma = 90°$, yielding 30% to 50% larger position errors. In summary, the results proved the necessity of customizing a measuring rod for a specific robot type, because a well-designed measuring rod can greatly improve MultiCal's performance.

After selecting the optimal measuring rod (125–500–90) in the real environment, we challenged MultiCal against the 6DM and 3DM methods in another calibration experiment. For the trial of the 6DM method, we employed a 6D binocular vision measuring system (Fig. 12, NDI Polaris Vega, accuracy $3\sigma = 0.2$ mm), which can measure both the position and orientation of a measuring marker. To better identify the kinematic parameters of the robot's wrist joint, the measuring marker was also installed using an offset mounting plate (the offset distance was 200 mm). Because we lacked a laser tracker that is commonly used to conduct the 3DM method, the above-described measurement method with the laser scanner was used instead, because the laser scanner used in this work has measurement accuracy (better than 43 μm) similar to a laser tracker. To attain the best performances of these devices, the optimal measurement configurations were selected using the above observability study. All of these devices and methods were evaluated with the validation method mentioned above.

To compare the sensitivities of these devices to the amount of measurement data, the calibration performances of different devices with 20, 30, and 40 measurement configurations were also tested separately. Furthermore, the actual time spent on the measurement processes t and the approximate cost of these devices were also compared. Considering that the time efficiency of the laser scanner is not comparable to those of other devices, we used the measurement time of the binocular vision system in the 6DM trial, which might be very close to that of a laser tracker, to evaluate the time efficiency of the 3DM method. The final results are presented in Table 4.

The results showed that the 3DM method using the laser scanner had the highest calibration accuracy and device cost in the experiment. The 6DM

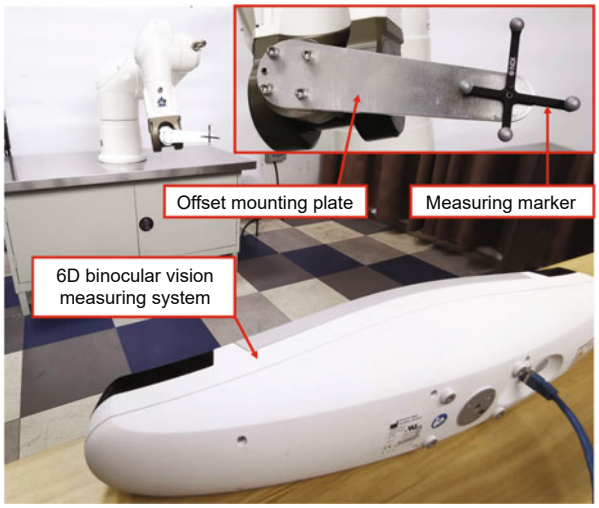

Fig. 12 Using a 6D binocular vision measuring system to implement the traditional calibration procedure based on 6D measuring (6DM) devices

Table 4 Comparison of different devices in terms of calibration accuracy, time efficiency, and approximate device cost

Device and number of configurations		Mean (mm)	Max (mm)	Standard deviation (mm)	t (min)	Cost (US$)
Laser scanner (3DM)	20	0.345	0.852	0.163	–	>50 000
	30	0.323	0.721	0.151	–	
	40	**0.302**	**0.707**	**0.145**	–	
Binocular vision (6DM)	20	0.841	1.786	0.441	12.5	>30 000
	30	0.714	1.517	0.353	18.2	
	40	0.616	1.434	0.301	24.1	
MultiCal	20	0.392	0.993	0.198	15.2	**<5000**
	30	0.348	0.869	0.156	23.5	
	40	0.339	0.831	0.151	30.5	

The bold number indicates the best performance

method with the binocular vision system had the poorest calibration accuracy, which may be due to its low measurement accuracy. In this trial, MultiCal had a 7% to 14% lower calibration accuracy compared to the laser scanner, and a 21% to 30% lower time efficiency compared to the binocular vision system. However, it significantly reduced the device cost. Additionally, MultiCal was slightly more sensitive to the amount of measurement data in contrast to 3DM, and had relatively poor performance with 20 measurement points.

Noted that the comparison of the device cost is relatively unfair because the cost of the prototype was compared against the selling price of those measuring devices. However, MultiCal can be easily fabricated at this cost. On the other hand, the MultiCal measurement procedure cannot be fully automated like TriCal and other traditional devices (such as laser trackers or camera-based systems), because it requires manual intervention to switch the mounting position of the measuring device (although it is very convenient when using the fast-lock mechanism). Thus, MultiCal has no advantage in large-batch calibration. However, for the application cases described in Section 1, the calibration frequency is not that high, but the calibration accuracy and the device cost would still be critical. In this sense, MultiCal still has a broad promotional prospect.

6 Conclusions

In this paper, we present a novel in-contact robot calibration device called MultiCal, which is accurate, low-cost, robust, and suitable for onsite calibration and online accuracy monitoring. MultiCal is based on the idea of using a long measuring rod and a multi-point constraint to obtain high calibration accuracy and robustness in the whole robot workspace. This advantage is quite competitive compared to most similar in-contact calibration devices, the calibration accuracy of which, in the workspace far from the measurement area, is relatively poor. We also prove the necessity of customizing a long measuring rod for a specific robot type, since a well-designed measuring rod can greatly improve MultiCal's calibration performance. In a comparative experiment, MultiCal with an optimal measuring rod presents a reduction of only 7% to 14% in calibration accuracy compared to a measuring arm with a laser scanner, and a reduction of 21% to 30% in time efficiency compared with a 6D binocular vision measuring system, yielding maximum and mean absolute position errors of 0.831 mm and 0.339 mm, respectively. Additionally, MultiCal can be easily fabricated at a low cost (less than US$5000).

However, the long measuring rod also brings the problem of rod deflection, leading to a decrease in measurement accuracy and limiting the application of MultiCal in larger robots. Hence, future work shall involve a more rigid structure for the measuring rod or a method to compensate for the deflection. In addition, the study of the optimal number and locations of the mounting positions in the multi-position fixture remains to be conducted.

Contributors

Ziwei WAN and Chunlin ZHOU designed the research. Ziwei WAN and Haotian ZHANG processed the data and drafted the paper. Jun WU helped organize the paper. Ziwei WAN and Chunlin ZHOU revised and finalized the paper.

Compliance with ethics guidelines

Ziwei WAN, Chunlin ZHOU, Haotian ZHANG, and Jun WU declare that they have no conflict of interest.

Data availability

The data that support the findings of this study are available from the corresponding authors upon reasonable request.

References

Castro HFF, Burdekin M, 2006. Calibration system based on a laser interferometer for kinematic accuracy assessment on machine tools. *Int J Mach Tools Manuf*, 46(2):89-97. https://doi.org/10.1016/j.ijmachtools.2005.05.001

Chen M, Hong X, Wei LS, et al., 2020. Robotic arm calibration and teaching method based on binocular vision. Proc 39th Chinese Control Conf, p.5963-5969. https://doi.org/10.23919/CCC50068.2020.9189529

Cho Y, Do HM, Cheong J, 2019. Screw based kinematic calibration method for robot manipulators with joint compliance using circular point analysis. *Robot Comput-Integr Manuf*, 60:63-76. https://doi.org/10.1016/j.rcim.2018.08.001

Cong DC, Yu DY, Han JW, 2006. Kinematic calibration of parallel robots using CMM. Proc 6th World Congress on Intelligent Control and Automation, p.8514-8518. https://doi.org/10.1109/WCICA.2006.1713640

Enebuse I, Foo M, Ibrahim BSKK, et al., 2021. A comparative review of hand-eye calibration techniques for vision guided robots. *IEEE Access*, 9:113143-113155. https://doi.org/10.1109/ACCESS.2021.3104514

Feng CS, Cong S, Shang WW, 2009. Integrated kinematic calibration for all the parameters of a planar 2DOF redundantly actuated parallel manipulator. *J Mech Robot*, 1(3):403-421. https://doi.org/10.1115/1.3147199

Gaudreault M, Joubair A, Bonev IA, 2016. Local and closed-loop calibration of an industrial serial robot using a new low-cost 3D measuring device. IEEE Int Conf on Robotics and Automation, p.4312-4319. https://doi.org/10.1109/ICRA.2016.7487629

Guo YX, Song B, Tang XQ, et al., 2020. A measurement method for calibrating kinematic parameters of industrial robots with point constraint by a laser displacement sensor. *Meas Sci Technol*, 31(7):075004. https://doi.org/10.1088/1361-6501/ab7bc1

Hayati S, Mirmirani M, 1985. Improving the absolute positioning accuracy of robot manipulators. *J Robot Syst*, 2(4):397-413. https://doi.org/10.1002/rob.4620020406

Icli C, Stepanenko O, Bonev I, 2020. New method and portable measurement device for the calibration of industrial robots. *Sensors*, 20(20):5919. https://doi.org/10.3390/s20205919

Ikits M, Hollerbach JM, 1997. Kinematic calibration using a plane constraint. Int Conf on Robotics and Automation, p.3191-3196. https://doi.org/10.1109/ROBOT.1997.606774

ISO, 1998. Manipulating Industrial Robots—Performance Criteria and Related Test Methods. ISO 9283:1998. International Organization for Standardization.

Joubair A, Bonev IA, 2015. Kinematic calibration of a six-axis serial robot using distance and sphere constraints. *Int J Adv Manuf Technol*, 77(1-4):515-523. https://doi.org/10.1007/s00170-014-6448-5

Joubair A, Nubiola A, Bonev I, 2013. Calibration efficiency analysis based on five observability indices and two calibration models for a six-axis industrial robot. *SAE Int J Aerosp*, 6(1):161-168. https://doi.org/10.4271/2013-01-2117

Legnani G, Tiboni M, 2014. Optimal design and application of a low-cost wire-sensor system for the kinematic calibration of industrial manipulators. *Mech Mach Theory*, 73:25-48. https://doi.org/10.1016/j.mechmachtheory.2013.09.005

Li BC, Shen J, 1991. Constrained optimization approach to the estimation of rotation matrix. *Robot*, 13(3):1-5 (in Chinese). https://doi.org/10.13973/j.cnki.robot.1991.03.001

Luo GY, Zou L, Wang ZL, et al., 2021. A novel kinematic parameters calibration method for industrial robot based on Levenberg-Marquardt and differential evolution hybrid algorithm. *Robot Comput-Integr Manuf*, 71:102165. https://doi.org/10.1016/j.rcim.2021.102165

Mitchell TJ, 1974. An algorithm for the construction of "D-Optimal" experimental designs. *Technometrics*, 16(2):203-210. https://doi.org/10.2307/1267940

Nubiola A, Slamani M, Joubair A, et al., 2014. Comparison of two calibration methods for a small industrial robot based on an optical CMM and a laser tracker. *Robotica*, 32(3):447-466. https://doi.org/10.1017/S0263574713000714

Park FC, Okamura K, 1994. Kinematic calibration and the product of exponentials formula. In: Lenarčič J, Ravani B (Eds.), Advances in Robot Kinematics and Computational Geometry. Springer, Dordrecht, p.119-128. https://doi.org/10.1007/978-94-015-8348-0_12

Qiao GX, Weiss BA, 2017. Accuracy degradation analysis for industrial robot systems. Proc ASME 12th Int Manufacturing Science and Engineering Conf Collocated with the JSME/ASME 6th Int Conf on Materials and Processing, Article V003T04A006. https://doi.org/10.1115/MSEC2017-2782

Sun T, Zhai YP, Song YM, et al., 2016. Kinematic calibration of a 3-DoF rotational parallel manipulator using laser tracker. *Robot Comput-Integr Manuf*, 41:78-91. https://doi.org/10.1016/j.rcim.2016.02.008

Sun T, Liu CY, Lian BB, et al., 2020. Calibration for precision kinematic control of an articulated serial robot. *IEEE Trans Ind Electron*, 68(7):6000-6009. https://doi.org/10.1109/TIE.2020.2994890

Sun Y, Hollerbach JM, 2008. Observability index selection for robot calibration. IEEE Int Conf on Robotics and Automation, p.831-836. https://doi.org/10.1109/ROBOT.2008.4543308

Zhan YB, 2015. Development of a Wire Draw Encoder Based Measurement System for Robot Calibration. MS Thesis, the Hong Kong University of Science and Technology, Hong Kong, China.
https://doi.org/10.14711/thesis-b1514478

Zhong XL, Lewis JM, Francis LNN, 1996. Autonomous robot calibration using a trigger probe. *Robot Auton Syst*, 18(4):395-410.
https://doi.org/10.1016/0921-8890(96)00011-5

List of supplementary materials